

ARTICLE

Received 12 Oct 2015 | Accepted 21 Mar 2016 | Published 9 May 2016

DOI: 10.1038/ncomms11369

OPEN

Spontaneous helix formation in non-chiral bent-core liquid crystals with fast linear electro-optic effect

Sithara P. Sreenilayam¹, Yuri P. Panarin^{1,2}, Jagdish K. Vij¹, Vitaly P. Panov¹, Anne Lehmann³, Marco Poppe³, Marko Prehm³ & Carsten Tschierske³

Liquid crystals (LCs) represent one of the foundations of modern communication and photonic technologies. Present display technologies are based mainly on nematic LCs, which suffer from limited response time for use in active colour sequential displays and limited image grey scale. Herein we report the first observation of a spontaneously formed helix in a polar tilted smectic LC phase (SmC phase) of achiral bent-core (BC) molecules with the axis of helix lying parallel to the layer normal and a pitch much shorter than the optical wavelength. This new phase shows fast ($\sim 30 \mu\text{s}$) grey-scale switching due to the deformation of the helix by the electric field. Even more importantly, defect-free alignment is easily achieved for the first time for a BC mesogen, thus providing potential use in large-scale devices with fast linear and thresholdless electro-optical response.

¹Department of Electronic and Electrical Engineering, Trinity College Dublin, The University of Dublin, Dublin 2, Ireland. ²School of Electrical and Electronic Engineering, Dublin Institute of Technology, Dublin 8, Ireland. ³Department of Chemistry, Martin Luther University Halle-Wittenberg, D-06120 Halle, Germany. Correspondence and requests for materials should be addressed to J.K.V. (email: jvij@tcd.ie) or to C.T. (email: carsten.tschierske@chemie.uni-halle.de).

Liquid crystals (LCs) are of significant importance for display applications, photonics, sensors, communication technologies and data processing systems. LCs used in industry, so far, are predominately nematics that consist of simple rod-like molecules¹. Disadvantages of nematic devices are their limited response time, failure to achieve RGB colour sequential display and a limited image grey scale. Faster switching is achieved with LC phases formed by chiral molecules, as, for example, blue phases², ferroelectric and antiferroelectric switching synclinal tilted (SmC^* , FLC) or anticlinical tilted smectic phases (SmC_A^* , AFLC)³. A new class of compounds with ferroelectric and antiferroelectric LCs is built from achiral bent-core (BC) molecules and has engendered great scientific interest in recent years⁴ due to a range of fascinating phenomena arising from the interplay of polarity and chirality^{5–7}. Unlike rod-like LCs, the BC compounds, even being achiral, may exhibit spontaneous polarization in the orthogonal (SmA -like)⁸ and tilted (SmC -like) smectic phases^{4,9}. In contrast to orthogonal BC phases^{10,11}, electro-optical effects can possibly be used for applications in tilted smectic phases of BCLC have not so far been reported, although electro-optical switching has been observed^{4,9,12}. A major reason is the impossibility to align these BC SmC phases. Besides these technological relevant aspects, spontaneous emergence of chirality in the tilted smectic phases of achiral BCLC is of prime general scientific importance^{13,14}. Chirality in the LC phases of BCLC results from the combination of tilt and polar order in the smectic phases (Supplementary Fig. 1)⁹ and was found for the so-called dark conglomerate phases^{5,13}, representing strongly distorted smectic phases with sponge-like structure¹⁵ or formed by helical nano-filaments¹⁶ and nano-size crystallites¹⁷. However, formation of smectic phases with helical superstructure having a helix axis parallel to the layer normal was not yet observed in the LC phases of any achiral BC mesogen^{5,6,18}.

Here we report the first experimental confirmation of formation of a helix in a polar SmC phase of achiral BC molecules with a pitch much shorter than the optical wavelength, showing fast ($\sim 30 \mu\text{s}$) grey-scale switching due to the deformation of the helix by the electric field. In contrast to other BC smectics, defect-free alignment is easily achieved, thus providing potential use in devices with fast linear and thresholdless electro-optical response.

Results

LC phases of compounds 1/*n*. BC materials under study are the two compounds 1/*n* of the homologue series of 4-cyanoresorcinol bisbenzoates with terephthalate-based wings and long *n*-alkyl chains ($n = 16, 18$) on both sides (Fig. 1a)^{11,19–21}. The synthesis of these compounds was performed as described in the Methods (Fig. 5). An identification of the phases, their transition temperatures and the enthalpy values for the two investigated compounds 1/*n* are given in Fig. 1a.

Transition temperatures were obtained on cooling under quasi-equilibrium condition with a rate of $\sim 1 \text{ K min}^{-1}$, whereas ΔH was taken from the DSC cooling curves (10 K min^{-1} , Supplementary Figs 2 and 3). On cooling a non-tilted and non-polar smectic (lamellar) LC phase (SmA) is formed first, which on further cooling transforms into a smectic phase with uniform (synclinal) tilt (SmC_s). This phase transition is observed optically by the occurrence of a birefringent Schlieren texture in the homeotropically aligned (optically uniaxial) SmA phase. The SmC phase is paraelectric and in the case of compound 1/16 changes into a $\text{SmC}_s\text{P}_F^{\text{hel}}$ helical synclinal ferroelectric phase with a short pitch and a helical axis lying parallel to the layer normal at $T = 110^\circ\text{C}$. For 1/18, a polar switching (synclinal ferroelectric)

SmC_sP_F phase (Supplementary Fig. 1) without helical superstructure is formed at this phase transition (at $T = 111^\circ\text{C}$); the $\text{SmC}_s\text{P}_F^{\text{hel}}$ phase is only formed after the application of an electric field, whereas SmC_sP_F is the stable ground state structure in this temperature range prior to the electric field having been applied. On further cooling, an antiferroelectric switching polar SmC phase (SmCP_A) is formed for both compounds below $T = 90^\circ\text{C}$. The polarization current curves recorded for the smectic phases of 1/18 under an applied triangular wave voltage are shown in the Supplementary Figs 6 and 10 and are discussed in detail in the Supplementary Note 1.

X-ray diffraction (XRD) patterns of aligned samples of the smectic phases of compounds 1/16 and 1/18 are shown in the Supplementary Figs 4 and 5, respectively. The diffraction patterns of both compounds are very similar and those of 1/18 are described here as an example of the case. There is a diffuse wide angle scattering with a maximum being shifted on cooling from $d = 0.47 \text{ nm}$ in the SmA phase to $d = 0.46 \text{ nm}$ in the SmC_sP_F phase (Fig. 1b, red dots). The diffuse character of the wide angle scattering confirms the LC state of the phases under discussion and the decreasing *d*-value indicates a growing packing density with decreasing temperature. A sharp small angle reflection corresponding to $d = 5.2 \text{ nm}$ appears in the SmA phase. It corresponds to 0.7 molecular length ($L_{\text{mol}} = 7.4 \text{ nm}$ in the most extended conformation between the ends of the alkyl chains in *all-trans* conformation), in line with a monolayer smectic phase. The *d*-value of the layer reflection increases with decreasing temperature, due to the alkyl chain stretching with growing packing density (Fig. 1b, black dots and Supplementary Table 2). The *d*-value even continues its growth at the SmA – SmC transition and in the SmC_s -range, reaching $d = 5.8$ – 6.0 nm in the SmC_sP_F phase. This means that, the effect of increasing packing density by alkyl chain stretching on the layer spacing is larger than the effect of developing the tilt. Indeed in the SmC_s phase an optical tilt of 18° is measured (Fig. 1c), which is relatively small compared with other bent-core mesogens where it is typically in the range of 35 – 45° (refs 5,6,18). Though the tilt is clearly confirmed by optical investigations, it is not evident from the XRD patterns, neither from the temperature-dependent development of the layer spacing nor from the positions of the wide angle with respect to the small angle scatterings in the two-dimensional (2D) XRD patterns of aligned samples, which is nearly orthogonal ($90 \pm 5^\circ$) at all temperatures (Supplementary Fig. 5). This indicates that the optical tilt of $\sim 18^\circ$ in the SmC_s phases mainly results from the tilt of the aromatic cores, whereas the more disordered aliphatic chains should be less tilted and preferably oriented opposite to the tilt direction of the aromatic cores. Similar results were obtained for compound 1/16 (Supplementary Fig. 4 and Supplementary Table 1), which have an even smaller optical tilt of 14° . This small tilt is assumed to be mainly due to the electron deficit terephthalate-based structure of the two rod-like wings attached to the 4-cyanoresorcinol core (Fig. 1a), which is known to support the formation of non-tilted or weakly tilted smectic phases^{22,23}.

Electro-optical investigations. Figure 2 presents the polarizing microphotographs in planar cells for 1/16 in Fig. 2a–e and for 1/18 in Fig. 2f–i, these are taken on cooling from the isotropic phase in the absence of an electric field. The planar cells were rotated at an angle $\alpha = 45^\circ$, where α is the angle between the rubbing direction, **R** and polarizer axis, **P**. The textures of the homeotropic cells are shown in the insets of Fig. 2. At 140°C (Fig. 2a,f) typical textures of both samples in planar cells correspond to a conventional uniaxial SmA phase with the optical axis lying along the rubbing direction **R**. The homeotropic textures

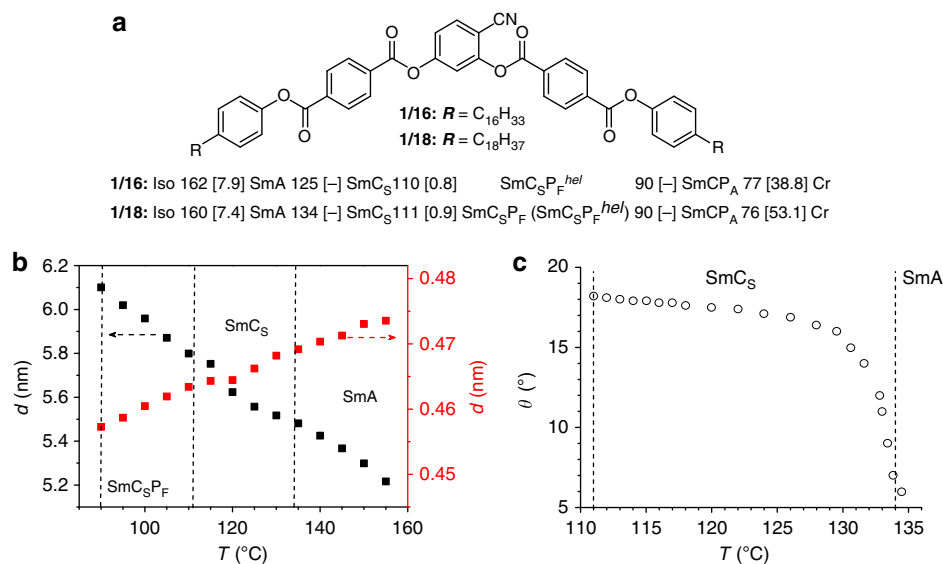


Figure 1 | Molecular structure and LC phases of 1/n. (a) Molecular structure and the phase sequences with transition temperatures (T (°C)) and transition enthalpies (ΔH (kJ mol⁻¹), in square brackets) as observed on cooling from the isotropic liquid state; Cr, solid crystal; Iso, isotropic liquid state; SmA, non-tilted and non-polar smectic (lamellar) LC phase; SmCP_A, antiferroelectric switching polar SmC phase; SmC_S, paraelectric smectic phase with uniform (synclinc) tilt; SmC_SP_F (synclinc ferroelectric LC phase, (Supplementary Fig. 1) and SmC_SP_F^{hel} helical synclinc ferroelectric phase with a short pitch and a helical axis lying parallel to the layer normal; SmCP_A, antiferroelectric switching polar SmC phase. For **1/18**, the parentheses indicate that the SmC_SP_F^{hel} phase is only formed after application of an electric field, whereas SmC_SP_F is the stable ground state structure in this temperature range prior to the field being applied. (b) Dependence of the d -values of the small angle scattering (black, left; layer thickness d follows the de Vries-like behaviour in tilted smectics) and the maximum of the wide angle scattering (red, right) on temperature in the XRD patterns of the smectic phases of compound **1/18**. (c) Temperature dependence of the optical tilt θ in the SmC_S phase of compound **1/18** as measured by rotating the LC sample in a 9 μ m planar cell under the polarizing optical microscope from the dark to the bright state (under an applied square-wave voltage of 40 V at 10 Hz, low frequency ac voltage is applied to minimize the effects of ions during switching).

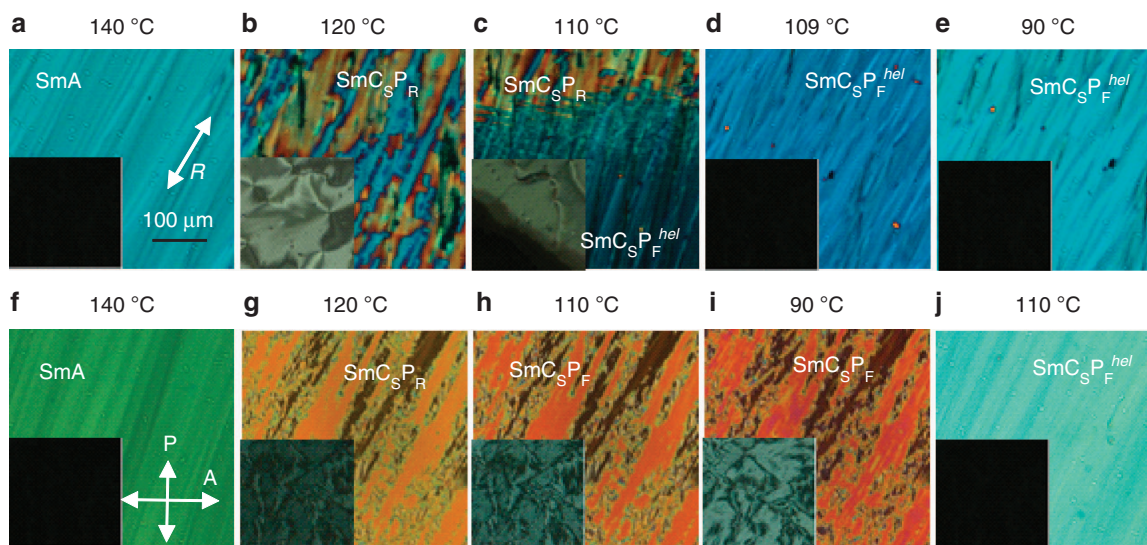


Figure 2 | Field-induced textural changes. Polarizing microphotographs (a–e) of compound **1/16** and (f–i) compound **1/18** of 6.5 and 8 μ m planar cells, respectively, taken on cooling from the isotropic phase. The insets show the corresponding textures of a 6.8 μ m homeotropic cell under the same conditions; a–i were taken in the absence of an external field, and (j) of **1/18** is obtained on the removal of the field after the cell was subjected to a square wave field (40 V_{pp}, $f = 110$ Hz) at $T = 110$ °C (h) with a corresponding homeotropic texture shown in the inset; **R** is the rubbing direction.

show perfect extinction, due to the orthogonal molecular organization in the layers (Fig. 2a,f, insets). On further cooling, the uniform texture breaks down into two sets of domains with an optical axis making an angle $\pm \theta_{app}$ with **R** (**1/16**: Fig. 2b; **1/18**: Fig. 2g), indicating the onset of a tilt which grows with a decrease

in temperature (Fig. 1c). The homeotropic textures show typical Schlieren textures due to this tilt (insets in Fig. 2b,g), in line with the formation of a synclinc SmC_S phase. The SmC_S phases, occurring in the temperature range between 134 and 111 °C for compound **1/18** and between 125 and 110 °C for the shorter

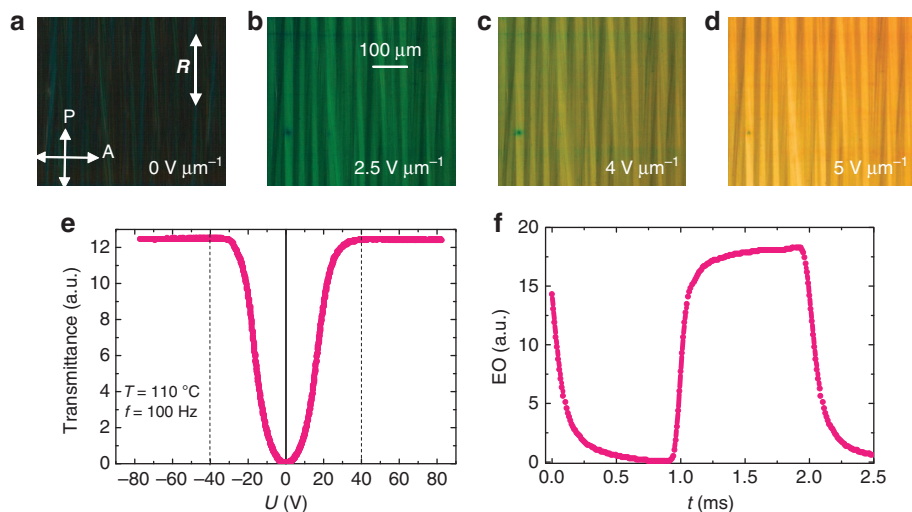


Figure 3 | Electro-optics in the $\text{SmC}_5\text{P}_F^{\text{hel}}$ phase of 1/18. Electro-optical investigations performed at 110°C on a $8\ \mu\text{m}$ planar cell. **a–d** show polarizing micrographs with sample in the field-induced $\text{SmC}_5\text{P}_F^{\text{hel}}$ phase (at $T = 110^\circ\text{C}$) taken at $\alpha = 0^\circ$ for different values of the electric field. R is the rubbing direction. **e** shows the optical response to an applied triangular voltage of $\pm 80\ \text{V}_{\text{pp}}$ ($\pm 10\ \text{V}\ \mu\text{m}^{-1}$) at $100\ \text{Hz}$ and **f** the electro-optical response to an applied square-wave $70\ \text{V}_{\text{pp}}$ voltage, for this experiment $\alpha = 22.5^\circ$.

homologue **1/16**, do not respond optically to the electric field. However, under a triangular wave voltage a single polarization current peak develops on approaching the phase transition at $T = 110/111^\circ\text{C}$, indicating the continuous growth of polar domains²⁴, in line with dielectric results (Supplementary Fig. 7). For both compounds, the colour of the texture of the planar cell gradually changes due to an increase in the birefringence following a typical increase in the orientational order parameter on cooling. On further cooling the cell with the compound **1/16** shows a transition to a uniaxial texture at $T = 110^\circ\text{C}$ (Fig. 2c,d), which looks rather similar to SmA but with a lower birefringence of the planar sample than in SmA (compare Fig. 2a,d). This uniaxial phase, designated as helical $\text{SmC}_5\text{P}_F^{\text{hel}}$ with a very short pitch persists down to $T = 90^\circ\text{C}$. In the phase designation ‘ P_F ’ stands for a uniform polar direction (ferroelectric order) and superscript ‘*hel*’ indicates the helical superstructure.

In contrast to the compound **1/16**, the textures of the planar cell for **1/18** do not show any principal changes at the phase transition at $T = 111^\circ\text{C}$, (Fig. 2g,h) while the colour of the planar cell gradually changes (Fig. 2g–i) due to a continuous increase in the birefringence. However, at 111°C weak electro-optical switching appears in response to the external electric field ($E = 0.9\ \text{V}\ \mu\text{m}^{-1}$) similar to the observations reported by Eremin *et al.*²⁵. On applying positive electric field, the optical axis of one type of domains switches to the right and the second domain switches to the left. The opposite is valid when negative electric field is applied. These features are typical for SmC_5P_F phases (Supplementary Fig. 8j–m).

The application of a square-wave electric field of amplitude $3\text{--}4\ \text{V}\ \mu\text{m}^{-1}$ to the SmC_5P_F phase of **1/18** causes an irreversible structural transition, that is, on the removal of the electric field the texture does not return to the initial state (Fig. 2h) but forms a uniaxial, low-birefringence texture (Fig. 2j) similar to the $\text{SmC}_5\text{P}_F^{\text{hel}}$ phase (Fig. 2d) observed in the compound **1/16** without application of an electric field (Supplementary Fig. 8a–i for details of the field-induced textures of **1/18**). Both textures are not only optically identical but also show similar electro-optical and other characteristics. Subsequent results and discussions are focused on **1/18** while at the same time these are applicable to **1/16** as well. It should be noted that textures of both samples on cooling in the absence of electric field show almost

perfect planar alignment (Fig. 2a,f) unlike textures obtained in previous studies of BC mesogens^{5,6}, where they consisted of focal conic defects. Such a good alignment had not previously been obtained.

Figure 3a–d shows the polarizing micrographs of **1/18** on a $8\ \mu\text{m}$ planar cell in the field-induced helical $\text{SmC}_5\text{P}_F^{\text{hel}}$ state, which exhibits the so-called V-shape switching. On the application of an electric field, the optical axis switches by a voltage-dependent angle $\pm\theta$ (V) from the rubbing direction with a corresponding gradual increase in the transmittance and birefringence (Fig. 3a–e), which saturates at $5\ \text{V}\ \mu\text{m}^{-1}$ with a uniform texture (Fig. 3d). A large value of the birefringence Δn_0 as in the non-helical virgin cell (Fig. 2h) is obtained.

Optical investigation of the switching process shows hysteresis-free and fully continuous EO response (Fig. 3e,f), apparent switching angle and the effective birefringence as a function of the field (Supplementary Fig. 8). This kind of continuous and thresholdless switching in tilted smectics was previously observed in helix-free and high P_S ferroelectric SmC^* phases²⁶, de Vries materials^{27,28} and FLC materials with short helical pitch due to electric field-induced deformed helix (DHFLC)²⁹, all requiring non-racemic chiral molecules, whereas the molecules considered here are achiral.

The remarkable feature of the $\text{SmC}_5\text{P}_F^{\text{hel}}$ phase is a texture of the homeotropic cell (Fig. 2j, inset) which shows a perfect extinction independent of the cell rotation angle between the crossed polarizers. This texture is similar to the uniaxial SmA phase (Fig. 2f), while all polar or non-polar SmC subphases show Schlieren textures (Fig. 2g–i, insets). The optically uniaxial structure in tilted phases is only possible for de Vries phases, SmC_α or helical structures with a helical pitch shorter than the wavelength of light. Both, de Vries and SmC_α phases, are very unlikely to exist because they both exhibit a strongly temperature-dependent saturation voltage²⁷, while in our study this is almost temperature independent over a relatively large temperature range of $20\ \text{K}$ (Supplementary Fig. 9). Thus, we conclude that the texture in Fig. 3 corresponds to a short-pitch helical structure of the $\text{SmC}_5\text{P}_F^{\text{hel}}$ phase.

Let us consider the physical reasons for the formation of a helix in non-chiral materials. According to the simple phenomenological theory developed by Pikin and Indenbom³⁰, the helical pitch

in chiral SmC^* phase can be expressed as:

$$q = \frac{2\pi}{p_0} = \frac{A + \mu P_S / \theta}{K} \quad (1)$$

where μ is the flexoelectric coefficient, P_S is the spontaneous polarization, θ is molecular tilt angle, K is the effective elastic constant and A is Lifshitz invariant, which is responsible for the formation of the helix of a certain sense due to the molecular chirality. This means that chiral SmC^* phase may form a helical structure even in the absence of spontaneous polarization. The existence of non-zero polarization shortens the helical pitch, while the sense of the helix is determined by the sign of A . In case of non-chiral molecules ($A=0$), the helical structure can be formed exclusively by soft matter with large spontaneous polarization. In other words, the formation of the helix reduces the electrostatic energy but increases the excess of elastic energy and the formation of helix of pitch $p_0 = 2\pi K\theta / \mu P_S$ is a compromise between these two competing terms. In the absence of the Lifshitz invariant, the two helices of opposite sense are equi-probable and this is being observed in our sample. The formation of very short sub-optical pitch (Supplementary Fig. 8) in our case can be explained by large P_S value ($\sim 300 \text{ nC cm}^{-2}$), a moderate tilt angle ($\sim 23^\circ$) (not shown in the Figure) and a reduced effective elastic constant due to the vicinity of anticlinic phase at a lower temperature.

It is known that the synchronization of helical conformers of non-chiral (but transiently chiral) molecules leads to spontaneous mirror symmetry breaking³¹, providing the chirality which determines the sign of A . Therefore, once formed, the helical structure stabilizes one of two possible molecular conformations due to the diastereomeric coupling between the helix sense and molecular conformations, that is, $A \neq 0$ and this additionally strengthens the helical organization with $q = \frac{A + \mu P_S / \theta}{K}$ and together with next-nearest-neighbor interactions³² further shortens the helix pitch, formed originally due to P_S . The existence of in-layer spontaneous polarization is also important in other liquid crystalline systems, for example, formation of ferroelectric subphases in AFLCs³³.

The observed electro-optical response to the applied electric field is similar to that of the deformed helical structure in SmC^* phases of highly chiral LCs (DHF effect)²⁹, which had attracted enormous interest at the time of its discovery for a potential application to fast-response LC devices with a tunable grey-scale. For compounds **1/n** in the $\text{SmC}_S\text{P}_F^{\text{hel}}$ phase, the switching time is found to be $\sim 30\text{--}40 \mu\text{s}$ and the contrast ratio of the electro-optical switching was found to lie between 200 and 300. It should be noted that all previously reported DHFLC studies were conducted only on chiral SmC^* phases of permanently chiral molecules with a large enough strength of the chirality. In contrast, the compounds used here are achiral and consequently these are more easily accessible when compared with highly chiral FLCs.

Due to the larger tilt, the layer coupling is stronger for **1/18**, which stabilizes the non-helical synclinic SmC_SP_F state where the helix is suppressed. In this case, a sufficiently strong electric field is required for its transition to the helical $\text{SmC}_S\text{P}_F^{\text{hel}}$ structure. The electric field improves ordering in the layers, leading to denser molecular packing, which is thought to support chirality synchronization of chiral conformers, thus supporting helix formation³¹. The $\text{SmC}_S\text{P}_F^{\text{hel}}$ state once formed appears to be stable in both homeotropic and planar cells. For both compounds **1/16** and **1/18**, the antipolar coupling increases with decreasing temperature, reaching a critical value at $\sim 90^\circ\text{C}$, when the SmCP_A phase is formed.

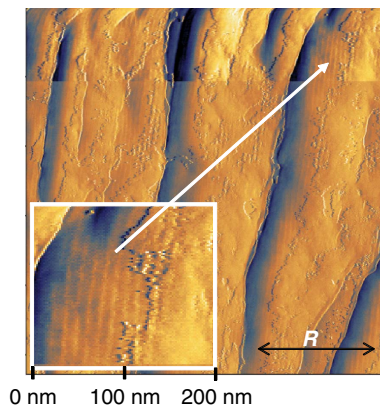


Figure 4 | AFM image of the $\text{SmC}_5\text{P}_F^{\text{hel}}$ phase in a planar cell. The $8 \mu\text{m}$ planar cell filled with **1/18** is used for AFM study. The helical ($\text{SmC}_5\text{P}_F^{\text{hel}}$) phase at 105°C was supercooled to the glassy state by immersing it into liquid nitrogen. Once supercooled, this material stays in the glassy state even at room temperature preserving the original structure of the phase under study. Then the glass plates of the LC cell were separated to enable the glassy material to be scanned by the AFM probe. The vertical stripes perpendicular to the rubbing direction **R** and smectic layer normal reveal a modulated structure corresponding to the helix.

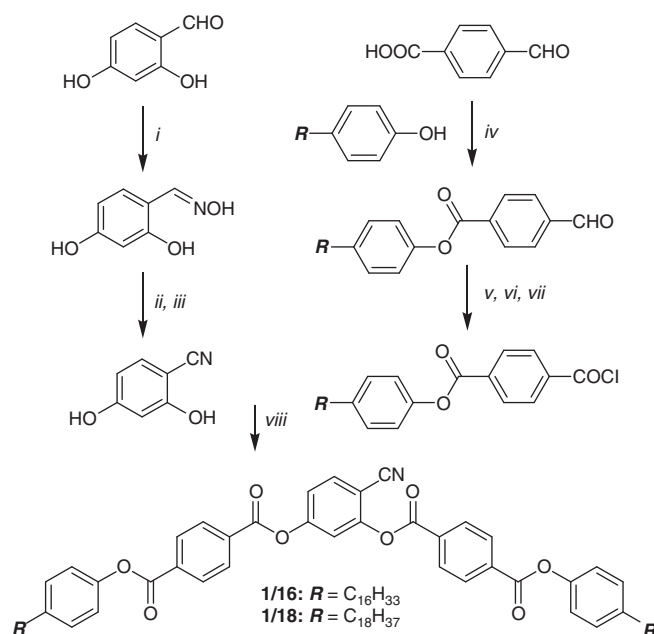


Figure 5 | Synthesis of compounds **1/n.** Reagents and conditions: (i) $\text{NH}_2\text{OH} \cdot \text{HCl}$, EtOH, Na_2CO_3 , 20°C , 6 h; (ii) Ac_2O , reflux, 3 h; (iii) KOH , H_2O , 20°C , 72 h; (iv) DCC , DMAP , CH_2Cl_2 , 20°C , 24 h; (v) NaClO_2 , NaH_2PO_2 , resorcinol; $t\text{-BuOH}$, 20°C , 12 h; (vi) HCl , H_2O , 20°C , 20 min; (vii) SOCl_2 , DMF , reflux, 1 h; (viii) Et_3N , cat. pyridine, CH_2Cl_2 , reflux, 6 h.

Atomic force microscopy. An evidence for the modulated helical superstructure in the SmC_SP_F phase is provided by the scanning of the sample by atomic force microscopy (AFM). The helical ($\text{SmC}_S\text{P}_F^{\text{hel}}$) phase of **1/18** at 105°C was super cooled to the glassy state by immersing it into liquid nitrogen. Once super cooled, this material stays in its glassy state³⁴ even at room temperature thus preserving its original structure. Then the glass plates of the LC cell were separated to access the glassy material by the AFM probe. Figure 4 shows an AFM image of the glassy **1/18** sample in the $\text{SmC}_S\text{P}_F^{\text{hel}}$ phase at room temperature. The vertical stripes

perpendicular to the rubbing direction \mathbf{R} and smectic layer normal reveal a modulated structure with a distance of ~ 14 nm, corresponding to approximately three layers. This provides a direct evidence for the existence of short-pitch helical structure with an angle $\sim 150^\circ$ between the \mathbf{C} -directors in neighbouring smectic layers similar to the model suggested by Pikin *et al.*³⁵. This pitch is at least 1 order of magnitude smaller than the minimal pitch detectable by optical techniques and this explains why the textures appear uniaxial in both homeotropic and planar geometries. This direct evidence supports our assumption of a helical structure in the $\text{SmC}_s\text{P}_F^{\text{hel}}$ phase.

Discussion

The structure of the SmC_sP_F phase in relation to possible SmC_AP_A , SmC_α and de Vries structures is being considered here. It would seem that the SmC_AP_A – SmC_sP_F transition in polar smectic phases of achiral BC mesogens is similar (structurally and electrically) to the electric field-induced SmC_A^* –to– SmC^* transition in chiral ferroelectric LCs of rod-like molecules. This process occurs through appearances of ferroelectric domains as dark/bright fringes parallel to the smectic layer normal. Such fringes grow in size with an increase in the electric field applied along the smectic layer normal to complete a uniform field-induced ferroelectric state³⁶, although there is a small linear pre-transitional effect³⁷. Therefore, the intermediate grey-scale during SmC_A – SmC transition is realized as a mixture of the antiferroelectric and ferroelectric domains (fringes) and electro-optic response must show both the voltage threshold and a strong hysteresis in the transmittance versus field. Most of the work on the BC systems as far as we are aware does not contain sufficient data on the intermediate states during the optical switching, with the exception of those given in refs 38,39, where the threshold, hysteresis and the fringes have been observed. In contrast to these observations our data show hysteresis-free (Fig. 3e) and complete analogue response, fringe-less change in the switching and hysteresis-free apparent optical tilt angle and the effective birefringence with field. Blinov *et al.*³⁹ have reported anomalously large pre-transitional effect in BC materials compared with the field-induced SmC_A^* – SmC^* switching, which gives about 20–25% of total apparent optical angle. Nevertheless, the rest of switching goes through fringes-domains and so on. Therefore, the continuous switching observed in our study is unlikely to be due to the SmC_AP_A – SmC_sP_F transition as was reported previously.

In the anticlinic SmC_AP phase, value of the effective birefringence is $\Delta n_{\text{eff}}(\theta) = \Delta n_0 \cos^2(2\theta)$, where Δn_0 is the birefringence of the field-induced synclitic SmC_sP state and for our case ($\theta = 18^\circ$, $\Delta n_0 = 0.1095$), $\Delta n_{\text{eff}}(\theta)$ equals 0.088. The effective birefringence of short-pitch helix is the same as for the de Vries type of SmA/SmC^* phases and depends on the tilt angle as: $\Delta n(\theta) = \frac{\Delta n_0}{2}(3 \cos^2(\theta) - 1)$ (ref. 40) and this gives a value of 0.094. The experimental value of 0.091 is exactly in between the two calculated values and hence both structures are plausible. Another strong argument in favour of de Vries and short-pitch helical structures is a texture of the homeotropic cell (Fig. 2j, inset) which shows a perfect extinction independent of the cell rotation angle between the crossed polarizers. This texture is similar to the uniaxial SmA phase (Fig. 2a), while all SmCP_A subphases show Schlieren (Fig. 2b–d, insets) textures. The optically uniaxial structure in tilted phases is only possible for de Vries phase or helical structures with a short sub-wavelength helical pitch. The first of the two, the de Vries phase is also ruled out because it shows a strongly temperature-dependent saturation voltage²⁷, while in our study this is almost temperature independent over a relatively large range of 20°C in

temperature (Supplementary Fig. 9). In addition, the two polarization peaks were also recorded in the SmC^*_α phases of chiral rod-like molecules⁴¹, having a similar short helical pitch superstructure as reported for the SmCP_α phase reported here for achiral BC molecules.

In conclusion, the spontaneous formation of a short-pitch helix in a tilted smectic phase of achiral BC LC is observed for the first time. This new helical LC phase ($\text{SmC}_s\text{P}_F^{\text{hel}}$) exhibits a linear electro-optic effect and shows fast grey-scale switching due to the deformation of the helix. The fast switching with temperature-independent tilt angle makes these non-chiral BC LCs not only perspective candidates for high-speed, grey-scale application in LCDs, light modulators and electro-optical shutters, but also it provides a new mode of spontaneous mirror symmetry breaking. Helix formation emerges at the onset of long range polar order in weakly tilted smectic phases. It is proposed that developing layer chirality, being the result of the orthogonal combination of tilt, polar direction and layer normal⁹, couples with conformational chirality of the achiral, but transiently chiral BC molecules^{13,31}. Interlayer helix formation obviously requires weak layer coupling as provided by compounds **1/16** and **1/18** having a relatively small synclitic tilt, whereas there is no indication of helix formation in any of the previously known polar SmC phases (B2 phases) of BC molecules, having much larger tilt angles and thus a stronger tilt correlation between the layers. Also in line with the proposed relation between layer coupling and helix formation, the $\text{SmC}_s\text{P}_F^{\text{hel}}$ phase is a stable phase for **1/16**, whereas **1/18**, having a slightly larger tilt and consequently a stronger layer coupling compared with **1/16**, forms the $\text{SmC}_s\text{P}_F^{\text{hel}}$ state only after application of a sufficiently strong electric field. Obviously, helix formation is associated with the nearly simultaneous emergence of tilt and polar order at the transition from the paraelectric SmC_s to the SmC_sP_F phase. Possibilities of this phase behaving similarly to de Vries tilted smectic or tilted SmC_α phase have been considered but these possibilities are being ruled out.

Methods

Synthesis. Compounds **1/n** were synthesized in-house according to the synthetic procedure shown in Fig. 5. Column chromatography was performed with silica gel 60 (63–200 μm , Fluka). Determination of structures and purity of intermediates and products was obtained by NMR spectroscopy (VARIAN Gemini 2000 and Unity Inova 500, VARIAN, all spectra were recorded at 27°C). Microanalyses were performed using a CARLO Erba-CHNO 1102 elemental analyzer and MALDI-TOF MS measurements were performed on a Bruker Autoflex III system (Bruker Daltonics) operating in reflection and linear modes; the matrix solution was prepared by dissolving *trans*-2-[3-(4-*tert*-butylphenyl)-2-methyl-2-propenylidene]malononitrile (DCTB, purchased from Sigma-Aldrich) in THF with a concentration of 20 mg ml^{−1}. The purity of all products was checked with thin layer chromatography (silica gel 60 F₂₅₄, Merck). $\text{CHCl}_3/\text{EtOAc}$ mixtures and $\text{CHCl}_3/\text{MeOH}$ mixtures were used as eluents and the spots were detected by UV radiation.

For the synthesis of compounds **1/n** the appropriate 4-(4-*n*-alkylphenoxy-carbonyl)benzoic acid (synthesized in analogy to the procedures given in ref. 42) (0.8 mmol) was refluxed in excess thionylchloride (25 ml) under argon atmosphere, after 1 h the excess thionylchloride was removed under vacuum, then 4-cyanoresorcinol⁴³ (54 mg, 0.4 mmol), triethylamine (0.07 ml, 0.52 mmol) and pyridine (0.05 ml) were dissolved in anhydrous CH_2Cl_2 (50 ml) and added to the acid chloride and stirring is continued under reflux for 6 h. The reaction mixture is then poured into aqueous 1 N HCl (10 ml). The organic layer was separated and washed twice with saturated aqueous NaHCO_3 solution. The combined aqueous layers were extracted with CH_2Cl_2 (30 ml). The organic extracts were dried over anhydrous Na_2SO_4 , filtered, and concentrated under vacuum. The crude products were purified by column chromatography using CHCl_3/n -hexane (9/1 V/V) as eluent followed by two crystallizations from ethanol/chloroform (9/1 V/V) mixture to give the desired final compound (**1/n**) as colourless crystals.

4-Cyano-1,3-phenylene bis[4-(4-hexadecylphenoxy-carbonyl)benzoate] (**1/16**).

Yield 83%. ¹H-NMR (500 MHz, CDCl_3): δ /p.p.m. 8.40–8.30 (m, 8H, Ar-H), 7.84 (d, ³*J*_{H–H} = 8.5 Hz, 1H, Ar-H), 7.61 (d, ⁴*J*_{H–H} = 2.1 Hz, 1H, Ar-H), 7.38 (dd, ³*J*_{H–H} = 8.5 Hz, ⁴*J*_{H–H} = 2.1 Hz, 1H, Ar-H), 7.27–7.21 (m, 4H, Ar-H), 7.15 (m, 2H, Ar-H), 7.14 (m, 2H, Ar-H), 2.67–2.60 (m, 4H, Ar-CH₂), 1.67–1.60 (m, 4H, CH₂), 1.37–1.22 (m, 52H, CH₂), 0.88 (t, ³*J*_{H–H} = 6.9 Hz, 6H, CH₃). ¹³C-NMR (101 MHz, CDCl_3):

$\delta/p.p.m.$ 164.08, 163.04, 162.72, 154.52, 153.22, 148.56, 148.53, 140.95, 140.89, 134.91, 134.79, 134.06, 132.55, 132.16, 130.60, 130.45, 130.38, 129.39, 129.37, 121.09, 121.06, 120.09, 117.23, 114.51, 104.57, 35.53, 32.06, 31.58, 29.83, 29.81, 29.73, 29.64, 29.49, 29.43, 22.83, 14.25. MALDO-TOF MS (m/z) [M + Na]⁺ calcd. for C₆₇H₈₅NO₈Na, 1054.6; found 1054.6; analysis (calcd. for C₆₇H₈₅NO₈) C 77.72 (77.95), H 8.13 (8.30), N 1.38 (1.36).

4-Cyano-1,3-phenylene bis[4-(4-hexadecylphenoxy)benzoate] (1/18).

Yield 58%. ¹H-NMR (500 MHz, CDCl₃): $\delta/p.p.m.$ 8.40–8.25 (m, 8H, Ar-H), 7.82 (d, ³J_{H-H} = 8.6 Hz, 1H, Ar-H), 7.59 (d, ⁴J_{H-H} = 2.2 Hz, 1H, Ar-H), 7.36 (dd, ³J_{H-H} = 8.5 Hz, ⁴J_{H-H} = 2.2 Hz, 1H, Ar-H), 7.23 (m, 4H, Ar-H), 7.13 (m, 2H, Ar-H), 7.12 (m, 2H, Ar-H), 2.67–2.54 (m, 4H, Ar-CH₂), 1.71–1.54 (m, 4H, CH₂), 1.38–1.18 (m, 60H, CH₂), 0.86 (t, ³J_{H-H} = 7.0 Hz, 6H, CH₃). ¹³C-NMR (126 MHz, CDCl₃): $\delta/p.p.m.$ 164.20, 163.13, 162.81, 154.56, 153.24, 148.57, 148.54, 141.01, 140.95, 134.89, 134.77, 134.12, 132.54, 132.15, 130.63, 130.48, 130.42, 130.42, 129.44, 129.42, 121.11, 121.08, 120.14, 117.26, 114.54, 104.51, 77.24, 35.39, 31.91, 31.46, 29.69, 29.67, 29.66, 29.59, 29.50, 29.35, 29.28, 22.68, 14.10. MALDO-TOF MS (m/z) [M + Na]⁺ calcd. for C₇₁H₉₃NO₈Na, 1110.7; found 1110.7; analysis (calcd. for C₇₁H₉₃NO₈) C 78.20 (78.34), H 8.57 (8.61), N 1.28 (1.29).

Optical and calorimetric investigations. Phase transitions were determined by polarizing microscopy (Leica DMR XP) in conjunction with a heating stage (FP 82 HT, Mettler) and controller (FP 90, Mettler) and by differential scanning calorimetry (DSC-7, Perkin Elmer) at heating/cooling rates of 10 K min⁻¹ (peak temperatures).

X-ray diffraction. XRD patterns of the aligned samples were recorded with a 2D detector (HI-STAR, Siemens or Vantec 500, Bruker). Ni-filtered and pin hole-collimated Cu-K_α radiation was used. Alignment was achieved by slow cooling (0.1 K min⁻¹) of a small droplet of the compound on a glass plate and took place at the sample–air interface. The sample to detector distance was 9.0 cm and 26.8 cm for the wide angle and small angle measurements, respectively, and the exposure time was 15 min.

Sample preparation for optical and electro-optical studies. The substrates of the planar cells for investigating the electro-optical response are coated with polymer RN 1175 (Nissan chemicals, Japan) and the coated surfaces are subsequently rubbed with a rotating commercial rubbing machine. The indium tin oxide (ITO)-coated glass substrates for the homeotropic cells are further coated with AL60702 polymer (JSR Korea). The gap between the electrodes for the in-plane field is 80 μm. The cell thickness was controlled by Mylar spacers of different thicknesses and the cell separation was measured by the optical interference technique. LC cells of these samples are studied using polarizing optical microscope (Olympus BX 52) equipped with an INSTEC's hot stage, temperature is controlled by Eurotherm 2,604 controller. The system is designed to obtain a temperature stabilization of the sample to within ±0.02°.

Dielectric spectroscopy. Dielectric relaxation measurements over a frequency range 1 Hz–10 MHz were performed using a broadband Alpha High Resolution Dielectric Analyser (Novocontrol GmbH, Germany). The glass substrates coated with low sheet resistance (20 Ω per square) ITO electrodes were used to make cells. The sheet resistance of the cell substrates is relatively low and thus the peak frequency due to the sheet resistance of the ITO in series with the capacitance of the cell is shifted to a frequency much higher than 1 MHz. The experimental set-up is calibrated by the prior measurements of the capacitance of the empty cell. The measurement is carried out under the application of weak field 0.1 V μm⁻¹. The temperature of the sample is stabilized within ±0.05 °C. The dielectric spectra are analysed using Novocontrol WINDETA programme. Temperature dependence of the dielectric strength ($\delta\epsilon$) and the relaxation frequency (f_R), are obtained by fitting the dielectric spectra to the Havriliak–Negami (H–N) equation:

$$\epsilon^*(\omega) = \epsilon' - i\epsilon'' = \epsilon_\infty + \sum_{j=1}^n \frac{\delta\epsilon_j}{[1 + (i\omega\tau_j)^{\alpha_j}]^{\beta_j}} - \frac{i\sigma_{dc}}{\epsilon_0\omega} \quad (2)$$

Here ϵ_∞ is the high frequency dielectric permittivity depending on the electronic and atomic polarizability, j is the number of relaxation processes required for the fit and it varies from 1 to n , $\omega = 2\pi f$ (frequency in Hertz) is the angular frequency, ϵ_0 is the permittivity in free space, τ_j is the relaxation time of the j^{th} relaxation process, $\delta\epsilon_j$ is the dielectric relaxation strength and α_j and β_j , respectively, are the symmetric and asymmetric broadening parameters of the j^{th} process related to the distribution of relaxation time. The $\sigma_{dc}/\epsilon_0\omega$ represents the contribution of dc conductivity to ϵ'' .

Atomic force microscopy. The structure of helical phase was studied by AFM on a Veeco Nanoscope-IIIa system (Digital Instruments). The samples for AFM study were prepared by filling 1/18 LC material in planar cells. The helical (SmC_P^{hel}) phase at 105 °C was super cooled to the glassy state by immersing it into liquid nitrogen. Once super cooled, this material stays in the glassy state even at room temperature preserving the original structure. Then the glass plates of the LC cell were separated to access the glassy material by the AFM probe.

References

- Bremer, M., Kirsch, P., Klasen-Memmer, M. & Tarumi, K. The TV in your pocket: development of liquid-crystal materials for the new millennium. *Angew. Chem. Int. Ed.* **52**, 8880–8896 (2013).
- Yan, J. *et al.* Polymer-stabilized optically isotropic liquid crystals for next-generation display and photonics applications. *J. Mater. Chem.* **21**, 7870–7877 (2011).
- Fukuda, A., Takanishi, Y., Isozaki, T., Ishikawa, K. & Takezoe, H. Antiferroelectric chiral smectic liquid crystals. *J. Mater. Chem.* **4**, 997–1016 (1994).
- Niori, T., Sekine, T., Watanabe, J., Furukawa, T. & Takezoe, H. Distinct ferroelectric smectic liquid crystals consisting of banana shaped achiral molecules. *J. Mater. Chem.* **6**, 1231–1233 (1996).
- Reddy, R. A. & Tschierske, C. Bent-core liquid crystals: polar order, superstructural chirality and spontaneous desymmetrisation in soft matter systems. *J. Mater. Chem.* **16**, 907–961 (2006).
- Takezoe, H. & Takanishi, Y. Bent-core liquid crystals: their mysterious and attractive world. *Jpn. J. Appl. Phys.* **45**, 597–625 (2006).
- Jakli, A., Nair, G. G., Lee, C. K., Sun, R. & Chien, L. C. Macroscopic chirality of a liquid crystal from nonchiral molecules. *Phys. Rev. E* **63**, 061710-1–061710-5 (2001).
- Reddy, R. A. *et al.* Spontaneous ferroelectric order in a bent-core smectic liquid crystal of fluid orthorhombic layers. *Science* **332**, 72–77 (2011).
- Link, D. R. *et al.* Spontaneous formation of macroscopic chiral domains in a fluid smectic phase of achiral molecules. *Science* **278**, 1924–1927 (1997).
- Shimbo, Y. *et al.* Ideal liquid crystal display mode using achiral banana-shaped liquid crystals. *Jpn. J. Appl. Phys.* **45**, L282–L284 (2006).
- Nagaraj, M., Panarin, Yu. P., Vij, J. K., Keith, C. & Tschierske, C. Liquid crystal display modes in a nontilted bent-core biaxial smectic liquid crystal. *Appl. Phys. Lett.* **97**, 213505-1–3 (2010).
- Heppke, G., Jakli, A., Rauch, S. & Sawade, H. Electric-field-induced chiral separation in liquid crystals. *Phys. Rev. E* **60**, 5575–5578 (1999).
- Tschierske, C. & Ungar, G. Mirror symmetry breaking by chirality synchronization in liquids and liquid crystals of achiral molecules. *Chem. Phys. Chem.* **17**, 9–26 (2016).
- Takezoe, H. Spontaneous achiral symmetry breaking in liquid crystalline phases. *Top. Curr. Chem.* **318**, 303–330 (2012).
- Hough, L. E. *et al.* Chiral isotropic liquids from achiral molecules. *Science* **325**, 452–456 (2009).
- Hough, L. E. *et al.* Helical nanofilament phases. *Science* **325**, 456–460 (2009).
- Alaasar, M., Prehm, M. & Tschierske, C. Helical nano-crystallite (hnc) phases—chirality synchronization of achiral bent-core mesogens in a new type of dark conglomerates. *Chem. Eur. J.* **22**, 6583–6597 (2016).
- Eremin, A. & Jakli, A. Polar bent-shape liquid crystals—from molecular bend to layer splay and chirality. *Soft Matter* **9**, 615–637 (2013).
- Sreenilayam, S. *et al.* Biaxial order parameter in the homologous series of orthogonal bent-core smectic liquid crystals. *Phys. Rev. E* **88**, 021504-1–021504-5 (2013).
- Panarin, Y. P., Nagaraj, M., Vij, J. K., Keith, C. & Tschierske, C. Field-induced transformations in the biaxial order of non-tilted phases in a bent-core smectic liquid crystal. *Europhys. Lett.* **92**, 26002-p1–p6 (2010).
- Keith, C., Prehm, M., Panarin, Y., Vij, J. K. & Tschierske, C. Development of polar order in liquid crystalline phases of a banana compound with a unique sequence of three orthogonal phases. *Chem. Commun.* **46**, 3702–3704 (2010).
- Pelzl, G. & Weissflog, W. in *Thermotropic Liquid Crystals: Recent Advances*. (ed. Ramamoorthy, A.) pp 1–58 (Springer, 2007).
- Alaasar, M. *et al.* Development of polar order and tilt in liquid crystalline phases of bent-core mesogens. *Soft Matter* **10**, 5003–5016 (2014).
- Alaasar, M., Prehm, M., Nagaraj, M., Vij, J. K. & Tschierske, C. A liquid crystalline phase with uniform tilt, local polar order and capability of symmetry breaking. *Adv. Matter* **25**, 2186–2191 (2013).
- Eremin, A. *et al.* Paraelectric–antiferroelectric transitions in the bent-core liquid-crystalline materials. *Phys. Chem. Chem. Phys.* **6**, 1290–1298 (2004).
- Clark, N. A., Coleman, D. & MacLennan, J. E. Electrostatics and the electro-optic behavior of chiral smectics C: 'block' polarization of applied voltages and 'V-shaped' switching. *Liq. Cryst.* **27**, 985–990 (2000).
- Panarin, Y. P., Panov, V., Kalinovskaya, O. E. & Vij, J. K. Observation of a possible random ferroelectric liquid crystal phase. *J. Mater. Chem.* **9**, 2967–2969 (1999).
- de Vries, A. The description of the smectic A and C phases and the smectic A–C phase transition of TCOOB with a diffuse-cone model. *J. Chem. Phys.* **71**, 25–31 (1979).
- Beresnev, L. A. *et al.* Deformed helix ferroelectric liquid crystal display: a new electrooptic mode in ferroelectric chiral smectic C liquid crystals. *Liq. Cryst.* **5**, 1171–1177 (1989).
- Pikin, S. A. & Indenbom, V. L. Piezoeffects and ferroelectric phenomena in smectic liquid crystals. *Ferroelectrics* **20**, 151–153 (1978).

31. Dressel, C., Reppe, T., Prehm, M., Brautzsch, M. & Tschierske, C. Chiral self-sorting and amplification in isotropic liquids of achiral molecules. *Nat. Chem.* **6**, 971–977 (2014).
32. Panarin, Y. P., Nagaraj, M., Sreenilayam, S., Lehmann, J. K. & Tschierske, C. Sequence of four orthogonal smectic phases in an achiral bent-core liquid crystal: evidence for the SmAP_z phase. *Phys. Rev. Lett.* **107**, 247801-1–247801-5 (2011).
33. Panarin, Y. P., Rosenblatt, Ch. & Aliev, F. M. Appearance of ferroelectric phases in a confined liquid crystal investigated by photon correlation spectroscopy. *Phys. Rev. Lett.* **81**, 2699–2702 (1998).
34. Gorecka, E. *et al.* Do the short helices exist in the nematic TB phase? *Liq. Cryst.* **42**, 1–7 (2015).
35. Pikin, S., Gorkunov, M., Kilian, D. & Haase, W. The semi-phenomenological model of antiferroelectricity in chiral smectic liquid crystals I. The structure of short pitch modes and a thermodynamical approach. *Liq. Cryst.* **26**, 1107–1114 (1999).
36. Wang, X. Y. *et al.* Kinetics of phase transition in an anticlinic liquid crystal induced by a uniform temperature field: growth in one dimension. *Phys. Rev. Lett.* **80**, 4478–4481 (1998).
37. Kimura, M., Kang, D. & Rosenblatt, C. Anticlinic coupling between layers of an antiferroelectric liquid crystal. *Phys. Rev. E* **60**, 1867–1871 (1999).
38. Weissflog, W. *et al.* Field-induced inversion of chirality in SmCP_A phases of new achiral bent-core mesogens. *J. Mater. Chem.* **15**, 939–946 (2005).
39. Blinov, L. M., Barnik, M. I., Bustamante, E. S., Pelzl, G. & Weissflog, W. Dynamics of electro-optical switching in the antiferroelectric B2 phase of an achiral bent-core shape compound. *Phys. Rev. E* **67**, 021706-1–021706-8 (2004).
40. Clark, N. A. *et al.* Electro-optic characteristics of de Vries tilted smectic liquid crystals: analog behavior in the smectic A* and smectic C* phases. *Appl. Phys. Lett.* **80**, 4097–4099 (2002).
41. Pandey, M. B., Dhar, R. & Dabrowski, R. Switching and dielectric behavior of SmC_z* phase. *Mol. Cryst. Liq. Cryst.* **547**, 74–80 (2011).
42. Alaasar, M., Prehm, M., Brautzsch, M. & Tschierske, C. 4-Methylresorcinol based bent-core liquid crystals with azobenzene wings—a new class of compounds with dark conglomerate phases. *J. Mater. Chem. C* **2**, 5487–5501 (2014).
43. Serrano, J. L. *et al.* Improving FLC properties. simplicity, planarity, and rigidity in new chiral oxazoline derivatives. *J. Am. Chem. Soc.* **117**, 8312–8321 (1995).

Acknowledgements

This work was supported by 13/US/I2866 from the Science Foundation of Ireland as part of the US–Ireland Research and Development Partnership program jointly administered with the United States National Science Foundation under grant number NSF-DMR-1410649 and by the DFG (Grant TS 39/24-1). We thank Prof. Hideo Takezoe (Toyota Physical and Chemical Research Institute, Japan) for the valuable discussions and suggestions. Also, we thank Beata M. Szydłowska (Trinity College Dublin) for assisting us in making the AFM measurements.

Author contributions

A.L. and M.Po. synthesized and purified the materials and performed optical and DSC investigations. M. Pr. performed XRD and interpreted the results. S.P.S., Y.P.P. and V.P.P. performed dielectric and electro-optical experiments and interpreted the results; Y.P.P., J.K.V. and C.T. supervised the work and have written the manuscript. All authors analysed and discussed the results and commented on the manuscript.

Additional information

Supplementary Information accompanies this paper at <http://www.nature.com/naturecommunications>

Competing financial interests: The authors declare no competing financial interests.

Reprints and permission information is available online at <http://npg.nature.com/reprintsandpermissions/>

How to cite this article: Sreenilayam, S. P. *et al.* Spontaneous helix formation in non-chiral bent-core liquid crystals with fast linear electro-optic effect. *Nat. Commun.* **7**:11369 doi: 10.1038/ncomms11369 (2016).



This work is licensed under a Creative Commons Attribution 4.0 International License. The images or other third party material in this article are included in the article's Creative Commons license, unless indicated otherwise in the credit line; if the material is not included under the Creative Commons license, users will need to obtain permission from the license holder to reproduce the material. To view a copy of this license, visit <http://creativecommons.org/licenses/by/4.0/>